Space/Time Structure of the Near-Surface Temperature Field During the NORPAX Pole Experiment[1]

T. P. BARNETT, R. A. KNOX AND R. A. WELLER

Scripps Institution of Oceanography, University of California, San Diego, La Jolla 92093

(Manuscript received 9 November 1976, in revised form 4 April 1977)

ABSTRACT

During January and February 1974 the NORPAX POLE experiment was carried out in the central Pacific to begin collection of data needed to design a large-scale ocean/atmosphere monitoring program. This paper describes features of the ocean temperature field observed during POLE within a region of about 400 km in diameter centered near 35°N, 155°W. The temperature field, which was approximately stationary during the month-long experiment, was dominated by a strong north-south gradient as expected. The east-west gradient was negligible. Superimposed on this mean field was energetic noise with typical rms isotherm displacements of 25 m near the bottom of the mixed layer. The characteristic horizontal scale of this noise was 50 km near the surface although the field appeared to be anisotropic. The energy, scale length and degree of anisotropy all decrease with depth. The implications of these observations to a sampling strategy are discussed as are other conclusions drawn from a statistical analysis of the temperature data.

1. Introduction

The POLE experiment was intended as a first step in gathering statistical information on relatively small horizontal and temporal scales of oceanic temperature variability so that an optimum thermal monitoring program could be established within NORPAX (North Pacific Experiment). In this paper we report observations of the temperature field, discussing in turn the methods and sampling scheme, the mean field configuration and statistics of the fluctuations. The relation of these items to generalized sampling considerations will be a main theme of the paper. In reading the paper it should be remembered that the results may not be representative of other regions and times. An example of this is given by comparing our results with the analysis of similar data obtained from the MODE area of the Atlantic.

Other results of the POLE experiment have been presented elsewhere: near-surface current profiles (Davis and Regier, 1974), direct air/sea flux measurements and comparisons with bulk aerodynamic formulas (Friehe and Schmitt, 1974, 1976), time series of temperature and salinity profiles at one location (Simpson, 1976), and a preliminary discussion of large-scale properties of the temperature field (Barnett and Rearwin, 1975). Additional analyses of the current data have been completed (Davis *et al.*, 1976).

[1] Authors listed alphabetically.

2. Observations and methods

The focus of POLE was the manned spar buoy R/P *Flip* (hence the name of the experiment), which was unanchored but remained near 35°N, 155°W. This site is in the North Pacific Current between the average positions of the subarctic and subtropical fronts (Roden, 1975). *Flip* carried out STD and current profiles, standard surface meteorological observations and direct air-sea flux experiments. The R/V *Thomas Washington* proceeded along various 200 km diameters of a circular region centered on *Flip* making alternate XBT and STD casts, to 450 and 500 m, respectively, at 10 km intervals. During the few periods of STD malfunction, XBT drops were substituted for the STD casts. A NAVOCEANO P-3 aircraft dropped calibrated AXBT probes at 40 km intervals along tracks covering the region described above. In addition, two 1000 km north-south sections were flown along both longitudes 155°W and 154°W. All observations were obtained between 26 January and 14 February, 1974. Fig. 1 shows the locations of the STD, XBT and AXBT profiles. In all, 166 STD's, 367 XBT's and 248 AXBT's were obtained from *Thomas Washington* and the P-3; these are the data discussed below.

On every third STD cast, Nansen bottles with reversing thermometers were placed at nominal depths of 0, 20, 100, 300 and 500 m, and the resulting data were used to calibrate the STD. Except for periods of obvious failure, the STD performed well, and a

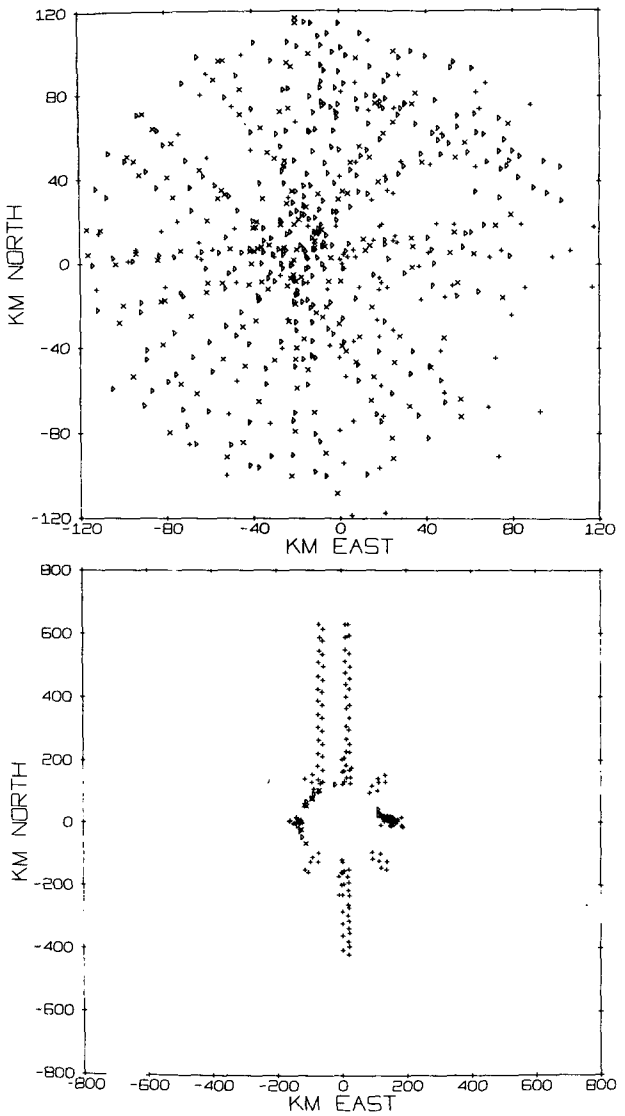

FIG. 1. Stations within 120 km of origin, which is at 35°N, 155°W (top) and stations farther than 120 km from origin (bottom). Symbols: +, AXBT; ×, STD; ▽, XBT.

simple correction scheme consisting of a constant offset in T and an S offset linearly increasing with depth sufficed to bring the errors within acceptable limits. The resulting error bounds (± 2 standard deviations) are ± 0.02°C and ± 0.01‰.

The XBT's exhibited a peculiar and disturbingly large error with respect to the (corrected) STD data. We did not have simultaneous XBT and STD casts to compare, because this technique would have cost us too many of our probes. Rather, the problem became evident when we averaged the XBT and STD temperatures over successive 25 m depth intervals and over all drops, and then computed the differences between these grand averages. The differences are large, as seen in Table 1. This calculation could return

TABLE 1. Comparison of depth-averaged XBT and STD temperatures. Superscripts denote average overall observations (1), and average over pairs of closely-spaced observations (2).

Depth interval (m)	${}^1T_{XBT}-{}^1T_{STD}$ (°C)	${}^2T_{XBT}-{}^2T_{STD}$ (°C)
0–25	0.36	0.36
25–50	0.36	0.33
50–75	0.41	0.36
75–100	0.52	0.50
100–125	0.59	0.56
125–150	0.36	0.40
150–175	0.28	0.36
175–200	0.26	0.35
200–225	0.28	0.35
225–250	0.31	0.39

nonzero differences if the instruments were accurate but the patterns of STD and XBT observations were not similarly placed in the mean temperature field, which is cooler to the north. In a second calculation, therefore, we selected close (usually within 10 km and 1 h) pair of XBT and STD drops, computed the temperature differences by depth interval for each pair, and averaged these differences. The results are much the same in either case (Table 1), and indicate that the XBT reads consistently high, with the worst error in the thermocline ($\sim$100 m). We are not certain of the source of this error although it may be due to a relatively slow XBT temporal response. In what follows we have subtracted a constant 0.38°C from all XBT temperatures prior to performing any computations. This brings the values to within ± 0.2°C of the STD.

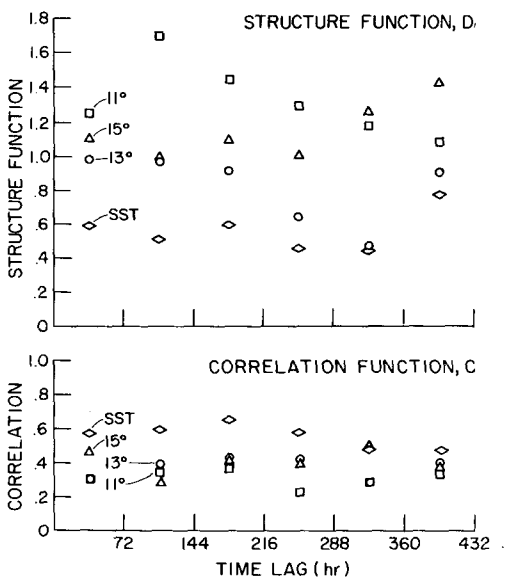

FIG. 2. Structure and correlation function of "nearby" AXBT isotherm depth pairs as functions of time lag.

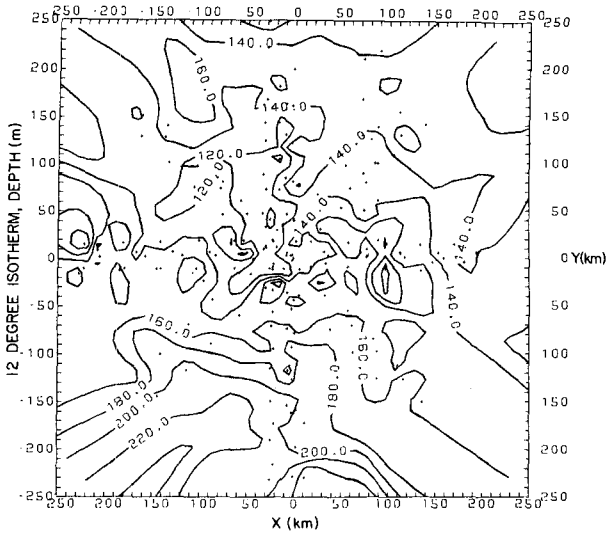

FIG. 3. Map of 12°C isotherm depth (m) from AXBT data. The + indicate a data point and the x-y coordinate system is centered on 35°N, 155°W.

The AXBT probes were individually calibrated before launch as described by Barnett and Sessions (1974) and Sessions *et al.* (1976). These authors show that calibrated AXBT's agree well with simultaneous hydrographic data. The resulting accuracy is conservatively estimated at ±0.2°C.

3. Mean field

In order to examine the mean configuration of the temperature field over the larger area sampled by the aircraft, the AXBT data were used to construct maps of isotherm depths. Before doing this we examined the time stationarity of the field by forming a series of all the spatially close (within 50 km) pairs of drops and computing the temporal structure and correlation functions for these pairs (after removing the mean). The results are shown in Fig. 2. Both functions are basically flat, i.e., closely spaced observations correlate about as well at short time lags as at long ones. We conclude that to a first approximation the AXBT data over the entire region can be lumped together for a single-time snapshot of the spatial structure of the field.

We then formed the contour maps of isotherm depths. Typical of these is the map for 12°C shown in Fig. 3. This isotherm *usually* lies near or slightly below the bottom of the mixed layer. There is a north-south slope of 90 m (500 km)$^{-1}$. The east-west slope is small and probably not significant. Small-scale features of 20–40 m amplitude are evident in the more densely sampled central portion of the region. Elementary statistics for this and other isotherms are given in Table 2.

The above results suggest several strategies/constraints in large-scale monitoring of the thermal field of the central Pacific. The strong north-south slope dictates that measurements to be averaged over a selected geographic area (e.g., a 5°×5° square) must be uniformly spaced in the north-south direction. Otherwise the sampling centroid will shift north-south and, working with the strong gradient, result in a biased estimate of the mean temperature of the averaging area. The large north-south slope and negligible east-west slope suggest that meridional sections, widely spaced in the zonal direction, will provide the most efficient monitoring network. Finally, the frequency of sampling will depend on the nature of the background noise, which appears to be rather large. We investigate the properties of this noise in the following section.

4. Fluctuations

a. Large-scale fluctuations

The large-scale spatial variability of the thermal field was investigated by estimating the structure function of the AXBT isotherm depth data according to

$$D(|\mathbf{r}|)=\langle[Z_T(\mathbf{x},t)-Z_T(\mathbf{x}+|\mathbf{r}|,t)]^2\rangle,$$

where Z_T is the depth of the isotherm for temperature T(°C) and $\mathbf{r}$ the separation vector between the observation points. The estimates of D assume stationarity over the duration of the experiment (Section 3) and are made as a function of $|\mathbf{r}|$ only, to

TABLE 2. Properties of large-scale mean temperature field and 95% confidence limits (error).

Isotherm (°C)	Mean depth (m)	Error (m)	North–South slope [m(100 km)$^{-1}$]	Error [m(100 km)$^{-1}$]	East–West slope [m(100 km)$^{-1}$]	Error (m(100 km)$^{-1}$]	Total variance (m^2)	Variance associated with North–South slope (%)
16	64	±13	−45	±10	−4	±15	1776	70
15	69	6	−20	6	3	7	1291	36
14	94	3	− 8	3	4	3	326	28
13	110	3	−11	3	0.8	3	444	40
12	148	4	−18	4	1	5	897	50
11	223	4	−11	3	−2	4	575	36
10	281	3	− 8	3	−3	3	364	41

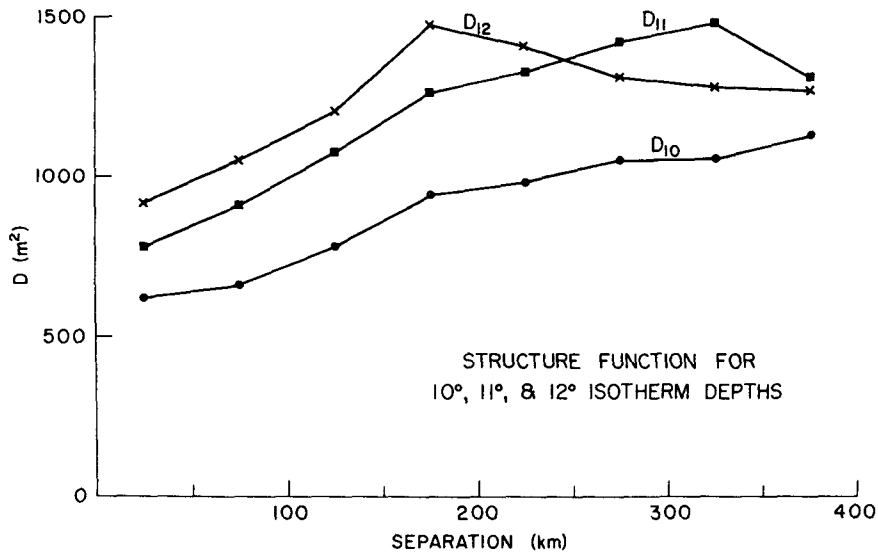

FIG. 4. Structure function D (m²) for three isotherm depths as estimated from AXBT data.

increase statistical reliability. The mean and linear least squares trends in latitude and longitude were removed prior to computing D. Typical results are shown in Fig. 4 and suggest the following conclusions:

1) Even for the closest separation the noise levels are quite high, thus indicating energetic, but small-scale, fluctuations in the thermal field. The noise is equivalent to an rms uncertainty in isotherm depth of 25–30 m. Any feasible climatological sampling scheme will have to contend with this high wave-number signal.

2) The small-scale signal attenuates with depth suggesting, as expected, that maximum variability occurs near the bottom of the mixed layer (typically the 12°C isotherm).

3) The steady rise of the structure function with increasing separation suggests a continuum of scales in the temperature field. However, the tendency of D to level off at greater separations suggests the presence of a minimum in the associated wave number spectrum. However, this speculation is based on very limited data.

TABLE 3. Parameters of least-squares fit of observed average temperatures to linear form $a+by+cx$, where y is the distance northward, x the distance eastward. For POLE $x=y=0$ at 35°N, 155°W. For MODE $x=y=0$ at 29°N, 68°W. σ is the standard deviation of residuals.

Layer		Pole	Mode
0–50 m	a	14.98 °C	21.42
	b	-5.175×10^{-3} °C km^{-1}	-1.215×10^{-3}
	c	-4.482×10^{-3} °C km^{-1}	5.116×10^{-4}
	σ	0.40 °C	0.33
50–100 m	a	14.37	20.76
	b	-4.975×10^{-3}	-5.060×10^{-4}
	c	-5.453×10^{-3}	6.645×10^{-4}
	σ	0.55	0.33
100–200 m	a	12.67	19.39
	b	-3.932×10^{-3}	1.433×10^{-3}
	c	-3.664×10^{-3}	1.676×10^{-3}
	σ	0.51	0.24
200–3000 m	a	10.57	18.28
	b	-3.325×10^{-3}	2.370×10^{-3}
	c	5.151×10^{-5}	2.079×10^{-3}
	σ	0.28	0.19
300–400 m	a	8.99	17.81
	b	-2.632×10^{-3}	3.334×10^{-3}
	c	3.140×10^{-4}	3.614×10^{-3}
	σ	0.32	0.26

It is informative to note that the rms isotherm displacement resulting from all scales of variability between 50–400 km is roughly equivalent to that associated with scales <50 km. This conclusion would have been substantially different had we not removed the strong north/south gradient from the field prior to computing D. This result also suggests the character of the small-scale noise is of crucial importance to the design of an optimum sampling program and, hence, its nature must be studied more closely (next section).

b. *Small-scale fluctuations*

In order to examine the finer scale structure of the field, the noise features of scale 0–50 km, we combined all the XBT and STD temperature profiles. This amounted to focusing on a region of about 100 km radius surrounding *Flip*, with observations at 10 km intervals; in contrast to the larger, coarser AXBT

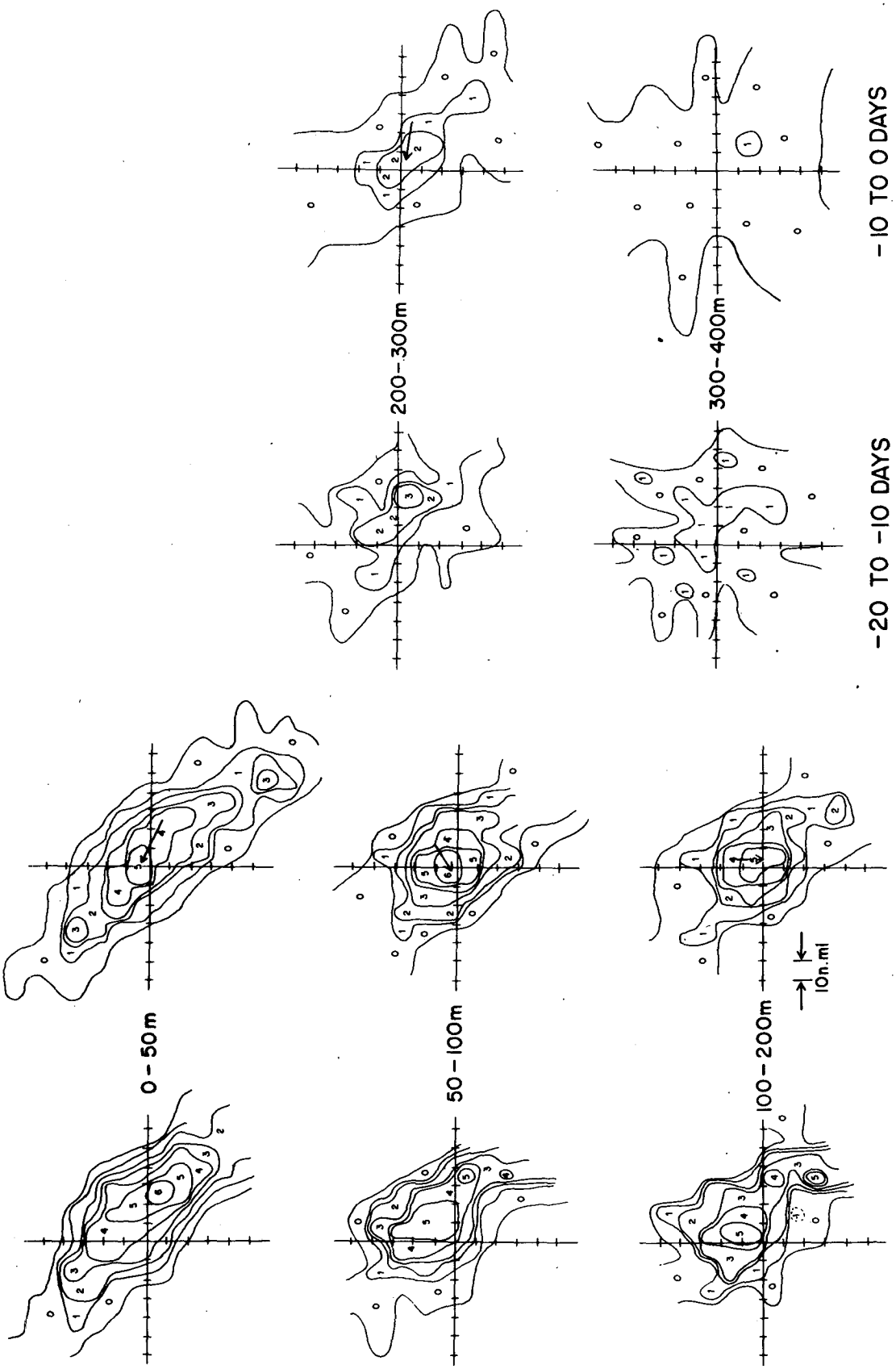

FIG. 5. Plots of POLE heat content correlation function for the five layers and two time lags indicated. The arrows indicate the direction and distance of displacement of the correlation function peak. The small numbers are the rounded values of correlation contours, e.g., 1 corresponds to a correlation of 0.10.

grid discussed above. We first calculated the space/time correlation functions of depths of selected isotherms, but these proved rather noisy. A clearer picture emerged if we considered the average temperature or heat content of various layers: 0–50 m, 50–100 m, 100–200 m, 200–300 m, 300–400 m. By a clearer picture we mean that the calculated correlation functions were smoother, with well-defined central maximum and zero contours. This is presumably due to the additional vertical averaging, which tends to filter out high-wavenumber fluctuations (internal waves?). We formed these averages from the individual profiles, subtracted a least-squares fit of the form $a+bx+cy$ (x=longitude, y=latitude) for each layer, and then calculated the space/time correlation function of the residuals at lag increments of 10 days and 18 km. The fit parameters and other elementary statistics are given in Table 3. Results are given in Fig. 5 in the form of contour plots of correlation function. For each level there are two plots, one for time lags between 0 and -10 days, and one for lags between -10 and -20 days. Referring to the 0–50 m layer, at 0 to -10 days, we see that the contours are elongated in the northwest-southeast direction. The distance from the central peak to the zero contour is ~190 km in this direction and ~56 km in northeast-southwest direction. At -10 to -20 days we see essentially the same pattern as regards orientation, scales and amplitude of the central peak, but the peak has moved as indicated by the arrow. The propagation or drift thus inferred is 5.5 km day^{-1} toward the *northwest*. This observation is in contrast to the eastward flow normally expected in this region.

This drift may be compared to the results from a set of drifting buoys launched during the experiment (Davis *et al.*, 1976). About 25 of these, drogued near the surface, resulted in useful tracks. The mean drift was 2.3 km day^{-1} northwestward. This is in the same direction as the drift of the correlation function pattern but at about half the speed. The drogues were concentrated in what proved to be the more slowly moving central portion of the region; a few drogues in the northwest quadrant had speeds as high as 9 km day^{-1}. This unbalanced geographical distribution may account for the lower estimate of mean speed from the overall collection of drogues.

In the 50–100 and 100–200 m layers we again have clearly defined central peaks surrounded by contours elongated northwest-southeast. But the details are not the same: The scale lengths to the zero contour are different or ill-defined, due to lack of data. The propagation or drift vectors are different for each of the layers: 2.6 km day^{-1} southwestward at 50–100 m, 2.6 km day^{-1} southward at 100–200 m. The amplitude in the central peak is not significantly decreased from that at 0–50 m, and thus this degree of correlation extends below the thermocline which typically lies at 80–100 m (Fig. 6).

Below 200 m, in the two deeper layers analyzed, the correlation amplitude drops abruptly, and the pattern becomes quite ragged. It is barely possible to discern a drift of 3.9 km day^{-1} westward for the layer 200–300 m. The 300–400 m layer shows only noise.

The sampling implications of the correlation functions shown in Fig. 5 are largely dictated by the typical value of 50 km for their first zero crossing.

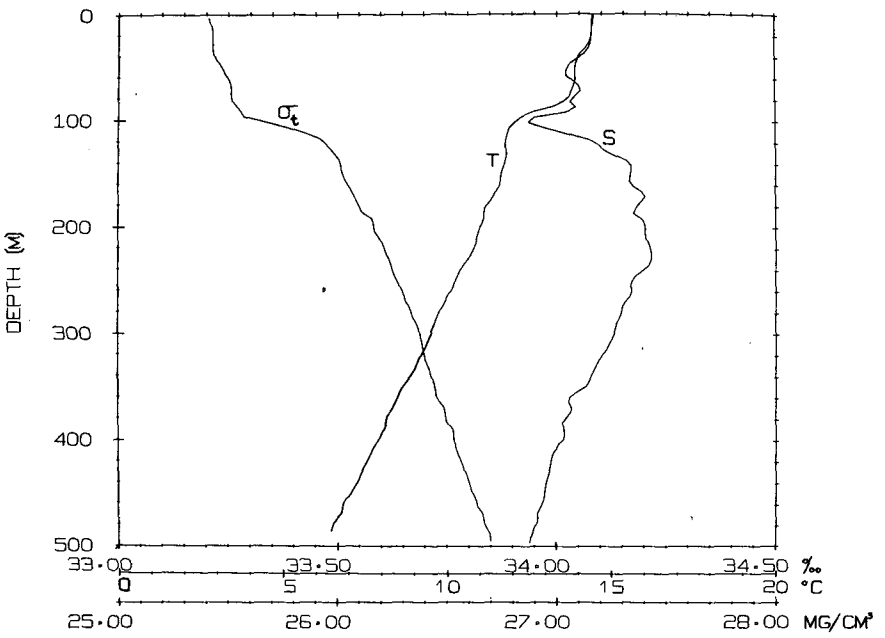

FIG. 6. Typical STD profile from POLE.

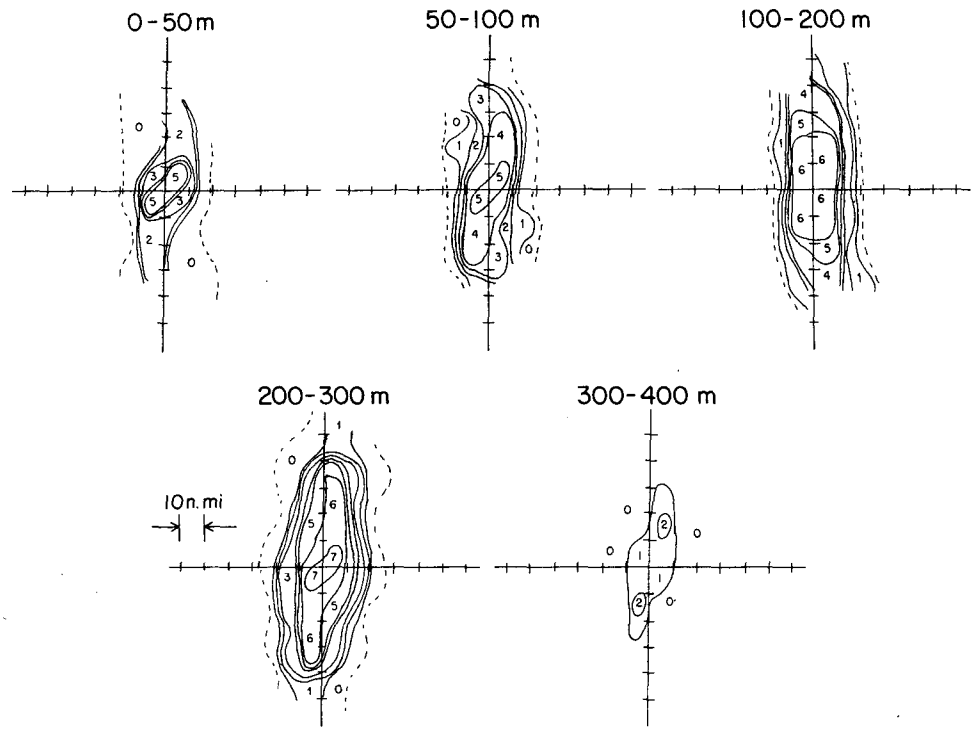

FIG. 7. Plots of MODE heat content correlation function.

This estimate, plus the simple procedures of Bayley and Hammersley (1946), suggest that a sampling interval of 75 km will provide highly efficient estimates of both mean isotherm depth and dispersion about that mean. The word "efficient" here refers to maximizing the ratio of the effective or independent number of observations to the total number of observations taken. A more extensive view of the sampling problem, which will not be undertaken here, should include errors associated with mapping the entire thermal field (e.g., Bretherton *et al.*, 1976).

5. Comparison with MODE XBT survey

As indicated in the Introduction, the results obtained during POLE are probably not representative of other oceanic regions. To illustrate the magnitude of the possible disparity we compare the present results with those obtained from a similar survey made during MODE.

During a one-week period in July 1973 an XBT survey consisting of 185 drops at roughly 10 km and 0.75 h spacing within a 2° square at 29°N, 68°W was carried out by Dr. D. W. Moore. We are grateful to him for furnishing these data and allowing us to analyze them. We have computed the correlation function for average temperature or heat content in the same manner and for the same layers as with the POLE data. Because of the limited number of samples, we have used only pairs within a single, centered time lag category (−2 to 2 days). This includes nearly all the data. The resulting contour plots are shown in Fig. 7. We make comparisons between these and the similar plots for the POLE data (Fig. 5), advancing some tentative explanations:

1) The MODE patterns are highly anisotropic, even more so than those of POLE. The scale in MODE is shorter; the semiminor axis in POLE (MODE) is 56 km (34 km) at 0–50 m, 60 km (34 km) at 50–100 m, 60 km (34 km) at 100–200 m and 60 km (49 km) at 200–300 m.

2) The magnitude of the correlation function at and near the central peak increases with depth in MODE, but decreases with depth in POLE, through the four shallowest layers. Just prior to the POLE experiment, a very strong winter storm passed through the area and it may be that the temperature signal we observed is a consequence of vigorous forcing on the (large) scale of the storm. The MODE data, on the other hand, were collected in summer in the absence of intense atmospheric forcing. One might then expect the near-surface temperature field above the shallow seasonal thermocline, which lies at about 100 m, to exhibit mostly small-scale features, or noise on the scale of the correlation computations presented here.

3) Both sets of data exhibit only noise in the 300–400 m layer. In the case of the MODE data, this is an abrupt change from the high correlation values at

200–300 m. We remark that 300–400 m is just at the depth of the so-called 18°C water, a quasi-homogeneous water mass with little lateral variability, either climatologically or during the MODE experment. Millard and Bryden (1973) have documented a minimum of temperature fluctuations in this depth interval from CTD profiles taken during MODE. In the POLE region no such permanent homogeneous layer exists (cf. Fig. 6); the noisy correlation field at 300–400 m occurs in the middle of a rather uniformly stratified portion of the water column.

6. Conclusions

The thermal field of the central Pacific, as observed during the POLE experiment, may be characterized as follows: 1) a strong north-south gradient dominated the field; 2) superimposed on this gradient was a highly energetic noise field with characteristic lengths scales of order 50 km or less; and 3) the energy associated with this small-scale noise was a maximum near the bottom of the mixed layer and attenuated slightly with increasing depth. The quantitative evaluation of the above items during POLE now makes it possible to define an optimized sampling program to observe large-scale thermal structure in the central Pacific Ocean. The methods for doing this may be found in Bretherton *et al.* (1976) among others.

High-resolution analysis of the temperature data suggests the existence of slowly propagating features in the near surface temperature field. The speed and direction of inferred propagation is in agreement with simultaneous drogue measurements (Davis *et al.*, 1976). Below 300 m, however, the analysis suggests the fluctuations in the thermal field are similar to those expected from a purely random process. A similar analysis of the MODE data shows somewhat different results. The largest signals are at depth suggesting the near-surface field is noisy. The differences may be attributed to the general oceanographic environment of the two study areas and to the dissimilar atmospheric forcing the areas experienced during the observing period.

Acknowledgments. We are indebted to Captain John Bonham and to the officers and crew of R/V *Thomas Washington* for the smooth operation of the ship in support of the STD and XBT observations. Thanks are due to Jeff Kerling and to the crew of the NAVOCEANO P-3 *El Coyote*, which flew the AXBT sections. Steve Rearwin and Meredith Sessions gave able assistance in AXBT data collection and processing. This work was supported by the Office of Naval Research under Contract N00014-69-A-0200, as part of the NORPAX program which is jointly sponsored by National Science Foundation Office of International Decade of Ocean Exploration and Office of Naval Research.

REFERENCES

Barnett, T. P., and M. H. Sessions, 1974: Characteristics of AXBT's. *NORPAX Highlights*, **2**, No. 6.

——, and S. Rearwin, 1975: Large-scale temperature and heat fields observed during POLE experiment. *NORPAX Highlights*, **3**, No. 2.

Bayley, G. N., and J. M. Hammersley, 1946: The "effective" number of independent observations in an autocorrelated time series. *J. Roy. Statist. Soc.*, **8**, No. 2 (Suppl.), 184–197.

Bretherton, F. P., R. E. Davis and M. Fandry, 1976: A technique for objective analysis and design of oceanographic experiments applied to MODE-73. *Deep-Sea Res.*, **23**, 559–582.

Davis, R. E., and L. A. Regier, 1974: Current meter profiling during POLE. *NORPAX Highlights*, **2**, No. 5.

——, T. P. Barnett and C. S. Cox, 1976: Variability of near surface currents observed during the POLE experiment. (In press.)

Friehe, C. and K. Schmitt, 1974: Estimates of surface fluxes during POLE. *NORPAX Highlights*, **2**, No. 5.

——, and ——, 1976: NORPAX POLE experiment micrometeorological results. *NORPAX Highlights*, **4**, No. 1.

Millard, R., and H. Bryden, 1973: Spatially averaged MODE-I CTD stations. *MODE Hot Line News*, **43**.

Roden, G., 1975: On North Pacific temperature, salinity, sound velocity and density fronts and their relation to the wind and energy flux fields. *J. Phys. Oceanogr.*, **5**, 557–571.

Sessions, M. H., T. P. Barnett and W. S. Wilson, 1976: The airborne expendable bathythermograph. *Deep-Sea Res.*, **23**, 779–782.

Simpson, J., 1976: The temperature and salinity structure of the upper ocean during the NORPAX POLE experiment. Paper presented Second Conference on Ocean-Atmosphere Interactions, Seattle, Amer. Meteor. Soc.